Computers, Materials & Continua
DOI: 10.32604/cmc.2023.032393
Article

Tech Science Press

An Algorithm to Reduce Compression Ratio in Multimedia Applications

Dur-e-Jabeen [1,*], Tahmina Khan[2], Rumaisa Iftikhar[1], Ali Akbar Siddique[1] and Samiya Asghar[1]

[1]Department of Electronic Engineering, Sir Syed University of Engineering & Technology, Karachi, Pakistan
[2]Department of Information & Computer Science, Sir Syed University of Engineering & Technology, Karachi, Pakistan
*Corresponding Author: Dur-e-Jabeen. Email: durejabeen@hotmail.com
Received: 16 May 2022; Accepted: 22 June 2022

Abstract: In recent years, it has been evident that internet is the most effective means of transmitting information in the form of documents, photographs, or videos around the world. The purpose of an image compression method is to encode a picture with fewer bits while retaining the decompressed image's visual quality. During transmission, this massive data necessitates a lot of channel space. In order to overcome this problem, an effective visual compression approach is required to resize this large amount of data. This work is based on lossy image compression and is offered for static color images. The quantization procedure determines the compressed data quality characteristics. The images are converted from RGB to International Commission on Illumination CIE La*b*; and YCbCr color spaces before being used. In the transform domain, the color planes are encoded using the proposed quantization matrix. To improve the efficiency and quality of the compressed image, the standard quantization matrix is updated with the respective image block. We used seven discrete orthogonal transforms, including five variations of the Complex Hadamard Transform, Discrete Fourier Transform and Discrete Cosine Transform, as well as thresholding, quantization, de-quantization and inverse discrete orthogonal transforms with CIE La*b*; and YCbCr to RGB conversion. Peak to signal noise ratio, signal to noise ratio, picture similarity index and compression ratio are all used to assess the quality of compressed images. With the relevant transforms, the image size and bits per pixel are also explored. Using the (n, n) block of transform, adaptive scanning is used to acquire the best feasible compression ratio. Because of these characteristics, multimedia systems and services have a wide range of possible applications.

Keywords: Color image; compression; color spaces; discrete orthogonal transforms (DOTs); peak-to-signal noise ratio (PSNR); similarity index

1 Introduction

The increasing number of choices for transferring and storing images via the internet has emerged from the continuous growth and advancement of digital apps [1]. Images include a large quantity of

data and cover a wide range of applications, including medical imagery, remote sensing, security, video conferencing, facial recognition, satellite communications and the environment and sustainability [2–7]. The visual data is made up of redundant and correlated pixels, which can be reduced using a sophisticated compression algorithm, resulting in smaller storage and transmission bandwidth [8]. The RGB model is widely used in color picture processing. The RGB color space is initially decorrelated with the use of an appropriate color conversion. This color space may contain additional color formats such as YCbCr, YUV, and International Commission on Illumination (CIE) La*b*;. It is desirable to modify the color space because the RGB components are inadequate for compression due to substantial inter-color dependency. The luma and chroma components of YCbCr are divided into image blocks [9]. In [10] the original RGB image is converted to YCbCr color space with discrete wavelet transform (DWT) and discrete cosine transform (DCT) applied to the Cb and Cr portions, respectively. Color spaces RGB, YCbCr, CIE La*b*;, and CIE Luv are examined for facial expression identification using a tensor perceptual color framework, with results favoring CIE La*b*; and CIE Luv in terms of robustness and performance. Clustering is possible in CIE La*b*; because a∗ and b∗ components represent the color element and the L component represents the brightness. CIE La*b*; is used for quantitative result evaluation in research aimed at eliminating the radiometric variance encountered in picture mosaicking [11].

Lossy methods can significantly reduce data size if the decompressed data is recovered within the acceptable boundaries set by each application. When opposed to its competing approach, lossy compression, lossless compression is used in situations that need correct retrieval and preservation of sensitive data at the cost of increased data size [9]. Initially Fourier Transform and DCT were preferred for image compression [12]. With time, several new techniques for image compression are offered including different variations of Wavelet Transform (WT) [13,14]. Medical imagery is preferred to be compressed by lossless algorithm for digital imaging and communications in Medicine [15]. Integer wavelet transform (IWT) is used [16] in conjunction with Huffman coding to compress images in area of telemedicine. This approach increases the magnitude of picture bit streams while lowering the signal to noise ratio (SNR). In [17], it describes a Discrete Fourier Transform (DFT) technique for compressing high Pixels Per Inch (PPI) photographs. An effective block-based lossless compression is proposed in [18] employing a Hadamard transformation on an image that has already been decomposed using IWT. While Discrete Cosine Transform (DCT) is widely used for image compression, Quantum DCT (QDCT), as explained in [19], is more efficient in terms of complexity than DCT.

The compression technique in this work is based on three color spaces, that is RGB, CIE La*b*; and YCbCr by applying seven discrete orthogonal transforms, namely Sequency Ordered–Complex Hadamard Transform (SCHT) [20,21], Conjugate Symmetric Sequency-Ordered Complex Hadamard Transform (CS-SCHT) [22], Natural ordered complex Hadamard Transform (NCHT) [23], Unified–Complex Hadamard Transform (UCHT) [24], Discrete Orthogonal–Complex Hadamard Transform (DOT-CHT) [25], Discrete Fourier Transform (DFT) [26] and Discrete Cosine Transform (DCT) [27]. In the RGB paradigm, determining a specific color is challenging. The fundamental advantage of the CIE La*b*; color space is that it is device independent. The findings suggest that the proposed CIE La*b*; algorithm outperforms alternative color spaces in detecting color. The YCbCr color space, unlike RGB, is brightness independent, which is why it performs better. Each obtained RGB image is also converted to YCbCr and CIE La*b*; color space. The different color planes of that image are compressed separately and then concatenated for the final image. The motivation behind this research is that to design and modify the quantization matrix in the transform domain in relation to various color models, as well as to find the optimal discrete orthogonal transform for color image

compression. The paper is organized into four sections: an introduction and literature review in Section 1, methodology in Section 2, results and conclusion in Sections 3 and 4, respectively.

2 Methodology

The extended method is developed for lossy color image compression, as previously stated. The compression is proposed and implemented utilizing multiple color spaces RGB, CIE La*b*, and YCbCr in the transform domain, in addition to numerous discrete orthogonal transformations (DOTs) such as SCHT, CS-SCHT, NCHT, UCHT, DOT-CHT, DFT, and DCT. According to the color model, the original image is passed via numerous color planes. For other models, the original RGB image is first converted into YCbCr and CIE La*b*. Before changing the image, all of the planes are split into R, G, B, L, a*, b*, Y, Cb and Cr with respect to the color model, as shown in Fig. 1. In terms of color space, the 8 × 8 DOT(s) are applied to each color plane. Lossy compression is achieved after thresholding and quantization, and a compressed image is received from the encoder. To restore the original image seen in Fig. 2, the decoder repeats the same inverse step. With respect to the various DOTs, Eqs. (1)–(3) present the different color planes into the transform domain (s).

$$\Psi_{r,L,Y}(k_1,k_2) = \frac{1}{NM}\sum_{n_1}^{N}\sum_{n_2}^{M}\xi_{R,L,Y}(n_1,n_2)\,H_N \tag{1}$$

$$\Psi_{g,\,a^*,\,Cb}(k_1,k_2) = \frac{1}{NM}\sum_{n_1}^{N}\sum_{n_2}^{M}\xi_{G,\,a^*,\,Cb}(n_1,n_2)\,H_N \tag{2}$$

$$\Psi_{b,\,b^*,\,Cr}(k_1,k_2) = \frac{1}{NM}\sum_{n_1}^{N}\sum_{n_2}^{M}\xi_{B,\,b^*,\,Cr}(n_1,n_2)\,H_N \tag{3}$$

where $\Psi_r(k_1,k_2)$, $\Psi_g(k_1,k_2)$, $\Psi_b(k_1,k_2)$, $\Psi_L(k_1,k_2)$, $\Psi_a(k_1,k_2)$, $\Psi_b(k_1,k_2)$, $\Psi_Y(k_1,k_2)$, $\Psi_{Cb}(k_1,k_2)$ and $\Psi_{Cr}(k_1,k_2)$ are the individually transformed planes in respective color space and DOTs. $\xi_R(n_1,n_2)$, $\xi_G(n_1,n_2)$, $\xi_B(n_1,n_2)$, $\xi_L(n_1,n_2)$, $\xi_a*(n_1,n_2)$, $\xi_b*(n_1,n_2)$, $\xi_Y(n_1,n_2)$, $\xi_{Cb}(n_1,n_2)$ and $\xi_{Cr}(n_1,n_2)$ are spatial domain color planes of respective color space with N and M number of rows and columns. H_N is the 8 × 8 different DOT(s) matrix to transform the color image into the transform domain. The three color spaces are applied and discussed below:

2.1 RGB Color Space

This color space is a display-oriented additive color model. Colors change depending on the color coordinates. On the basis of channel or plane, color picture compression is performed on each pixel of the image. As a result, color details and sharpness are diminished, potentially resulting in the loss of residual information in the form of tiny color details.

*2.2 RGB to CIE La*b*; Transformation*

After converting from one color space to another, compression is done on several planes to ensure that the color is lost as little as possible. The image is transformed from RGB to CIE La*b*; transformation before applying the DOT(s). Converting RGB to XYZ coordinates is required for CIELa*b*; [9,28]:

$$XYZ = \begin{bmatrix} 0.412453 & 0.357580 & 0.180423 \\ 0.212671 & 0.715160 & 0.072169 \\ 0.019334 & 0.119193 & 0.950227 \end{bmatrix} \begin{bmatrix} R \\ G \\ B \end{bmatrix} \tag{4}$$

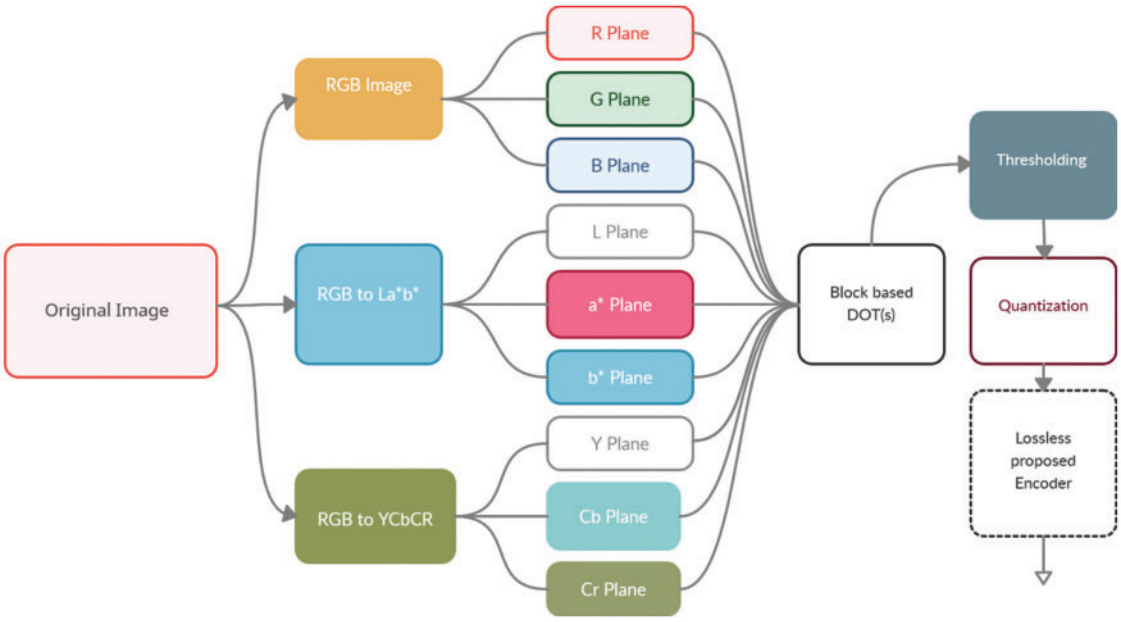

Figure 1: Encoding process for compression

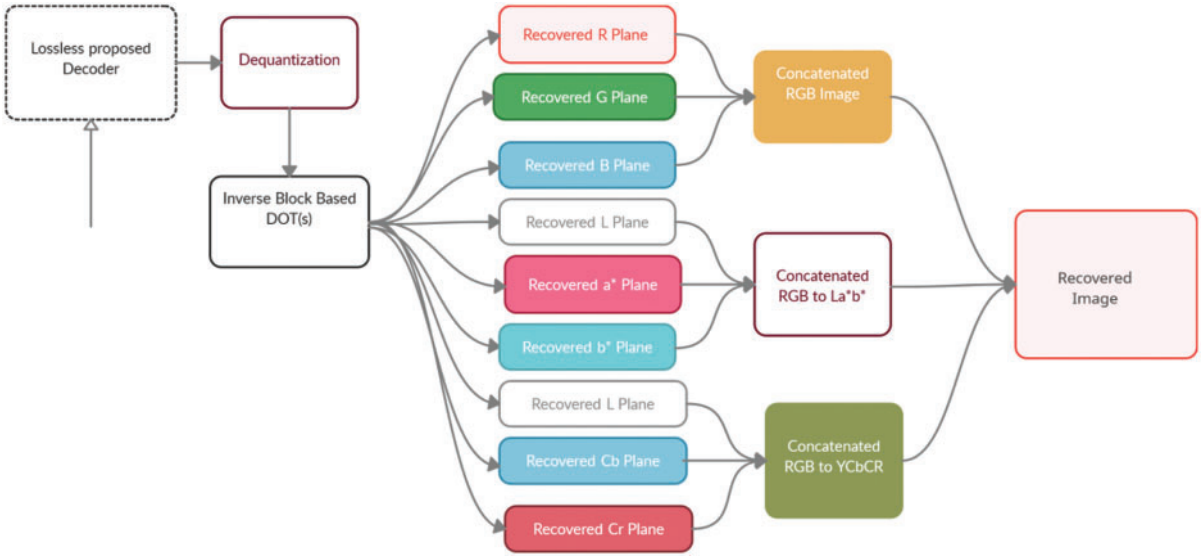

Figure 2: Decoding process for the lossy compression

The CIELa*b*; coordinates are extracted from XYZ as below:

$$L^* = 116f\left(\frac{Y}{Y_n}\right) - 16 \tag{5}$$

$$a^* = 500\left(f\left(\frac{X}{X_n}\right) - f\left(\frac{Y}{Y_n}\right)\right) \tag{6}$$

$$b^* = 200\left(f\left(\frac{Y}{Y_n}\right) - f\left(\frac{Z}{Z_n}\right)\right) \tag{7}$$

2.3 RGB to YCbCr Transformation

It has been observed that the YCbCr provides a better compression ratio without dropping the information [9]. The RGB image is converted in to the YCbCr before applying the DOT(s):

$$\begin{bmatrix} Y \\ C_b \\ C_r \end{bmatrix} = \begin{bmatrix} 0.299 & 0.587 & 0.144 \\ -0.16875 & -0.33126 & 0.5 \\ 0.5 & -0.41869 & -0.08131 \end{bmatrix} \begin{bmatrix} R \\ G \\ B \end{bmatrix} \underset{\text{Invese}}{\longleftrightarrow} \begin{bmatrix} R \\ G \\ B \end{bmatrix} = \begin{bmatrix} 1 & 0 & 1.402 \\ 1 & -0.34413 & -0.71414 \\ 1 & 1.772 & 0 \end{bmatrix} \begin{bmatrix} Y \\ C_b \\ C_r \end{bmatrix} \tag{8}$$

The energy of each plane of the three color spaces are expressed below:

$$E_{R,G,B} = \left(\frac{\sum_{n=0}^{N}\sum_{m=0}^{M} R_{n,m}^2 \text{ or } G_{n,m}^2 \text{ or } B_{n,m}^2}{E_{Total\_RGB}}\right) \times 100 \tag{9}$$

$$E_{L,a*,b*} = \left(\frac{\sum_{n=0}^{N}\sum_{m=0}^{M} L_{n,m}^2 \text{ or } a_{n,m}^2 \text{ or } b_{n,m}^2}{E_{Total\_Lab}}\right) \times 100 \tag{10}$$

$$E_{Y,Cb,Cr} = \left(\frac{\sum_{n=0}^{N}\sum_{m=0}^{M} Y_{n,m}^2 \text{ or } Cb_{n,m}^2 \text{ or } Cr_{n,m}^2}{E_{Total\_YCbCr}}\right) \times 100 \tag{11}$$

Total energy is defined as below:

$$E_{Total} = \left(\sum_{n=0}^{N}\sum_{m=0}^{M} P1_{n,m}^2\right) + \left(\sum_{n=0}^{N}\sum_{m=0}^{M} P2_{n,m}^2\right) + \left(\sum_{n=0}^{N}\sum_{m=0}^{M} P3_{n,m}^2\right) \tag{12}$$

The color planes of each color space are P1, P2 and P3. In Tab. 1, energy distribution of each plane is shown. The energy distribution confirms that color space conversion from RGB to CIELa*b* and YCbCr is required to achieve concrete results, whether for isolated or combined images (as an average).

Table 1: RGB, CIE La*b* and YCbCr color spaces energy distribution in each plane.

Image	E_R	E_G	E_B	E_L	E_{a^*}	E_{b^*}	E_Y	E_{Cb}	E_{Cr}
Airplane	31.7410	31.8396	36.4194	99.6588	0.0758	0.2654	99.8487	0.1503	0.0011
Peppers	55.7964	33.1998	11.0038	87.5003	1.4355	1.0643	91.0845	5.8188	3.0967
Lenna	60.8216	18.3719	20.8065	90.5558	9.2735	0.1707	89.3751	0.6004	1.0245
Girl	41.0989	32.3343	26.5667	98.1201	1.0845	0.7954	99.0356	0.3877	0.5767
Couple	51.5533	26.3603	22.0863	95.0304	3.9036	1.0660	95.2543	0.6612	4.0845
House	33.2403	38.9358	27.8240	98.5116	0.4011	1.0873	99.5234	0.4217	0.0549
Baboon	39.1006	34.3948	26.5046	98.7735	0.0012	1.2253	99.2971	0.4717	0.2312
Zelda	51.5533	26.3603	22.0863	95.0304	3.9036	1.0660	95.2543	0.6612	4.0845
Sailboat	37.4612	33.7263	28.8125	98.6677	0.5367	0.7956	99.6700	0.1841	0.1459
Average	**44.7074**	**30.6137**	**24.6789**	**95.7610**	**2.2906**	**1.9484**	**96.4826**	**1.0397**	**2.4778**

2.4 Proposed Quantization

The quantization matrix determines the compressed image quality (Qm). To provide the needed compressed image quality, the standard Qm is adjusted. The human eye is more sensitive to the brightness component of a color image than the chroma component, according to research. As a result, increasing the operating Qm reduces the image chrominance effect while maintaining overall quality.

In the suggested and designed algorithm, a standard JPEG Qm is a primary model and modified using Eq. (13):

$$\mathfrak{F}_{Qm} = \sum_{n=0}^{N} \sum_{m=0}^{M} \left(\frac{\left(\sum_{m=0}^{M} \Re\,(k, m) \right) \; Qm(n, m)}{\mathfrak{P}\; Max\left(\left(\sum_{m=0}^{M} \Re\,(k, m) \right) \right)} \right) \tag{13}$$

In a modified quantization matrix is $\mathfrak{F}_{Qm}$, the sum of the column vector of the transformed plane is $\sum_{m=0}^{M} \Re\,(k, m)$, $\mathfrak{P}$ is a crisp parameter that varies from 1 to 25 to maintain the quality of the image [29]. If $\mathfrak{P}$ is less than 1, the image quality deteriorate therefore it is never equal to zero. Fig. 3 shows the process of the modified quantization matrix.

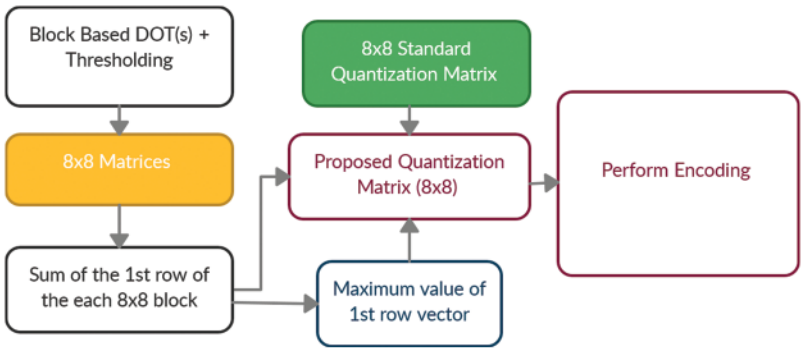

Figure 3: Proposed quantization matrix

2.5 Block Based DOT(s)

The color planes are split for the appropriate color space, and each plane is transformed in 8×8 blocks with respect to the transformation matrix and quantized with the appropriate DOT(s), such as (SCHT, CSSCHT, NCHT, UCHT, DOTCHT, DFT, and DCT), and new coefficients for each DOT are obtained. Similarly, decompression is performed, and the compressed picture is received at the decoder side.

3 Experimental Results and Comparison

The standardized test images "Airplane, Baboon, Couple, Girl, House, Lena, Peppers, and Sailboat" are used to test the improved quantization matrix in the frequency domain, as shown in Fig. 4. Different DOT(s) are applied such as SCHT, CS-SCHT, NCHT, UCHT, DOTCHT, DFT and DCT in numerous color spaces are applied such as RGB, CIE La*b*;, and YCbCr. In the frequency domain, several metrics such as PSNR, SNR, Compression ratio, BPP, SI and file size are analyzed to determine compression quality and efficiency. The performance of the modified quantization matrix that is applied during compression for the various DOTs is shown in Tabs. 2–8. The 8×8 block size is applied with respect to the quantization matrix after preparatory processes of color domain conversion

for the various color spaces. Experiments are performed with different "$\mathfrak{P}$" values ($\mathfrak{P}$ = 1, 5, 10, 15, 20, 25). Fig. 5 presents the qualitative analysis of the compression comparison for the DOTs with $\mathfrak{P}$ = 1 for all the test images. Fig. 6 shows the measurable outcomes of the PSNR for the "airplane" image using DOTs and color spaces.

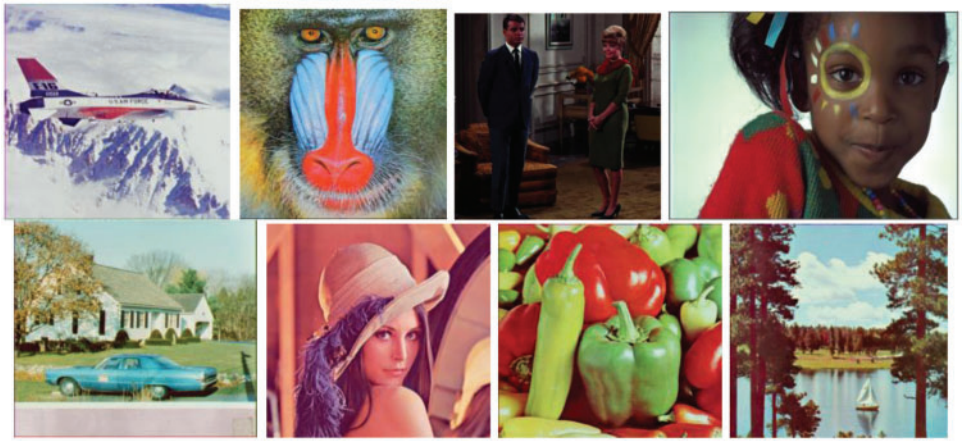

Figure 4: Original images: Airplane, baboon, couple, girl, house, lena, peppers and sailboat respectively

Table 2: Performance of RGB, CIE La*b* and YCbCr color spaces in SCHT with Quantizer Width $\mathfrak{P}$ = 1

SCHT - RGB at Quantizer Width $\mathfrak{P}$ = 1						
Images	PSNR	SNR	Compression ratio	BPP	Similarity index	File size (KB)
Airplane	36.4522	11.8092	29.0613	0.8258	0.8382	27.066
Peppers	37.4503	15.5456	27.7617	0.8645	0.9583	28.333
Lena	37.7558	14.9086	10.7745	2.2275	0.9597	25.17
Girl	37.2049	17.9717	28.1074	0.8539	0.8944	22.186
Couple	36.9359	10.2608	29.4577	0.8147	0.8062	6.679
House	35.1419	12.2497	22.9596	1.0453	0.8764	34.259
Baboon	32.9596	8.8416	16.5194	1.4528	0.7611	47.615
Sailboat	36.4818	13.2382	21.9823	1.0918	0.8799	35.782
SCHT – CIE La*b*; at Quantizer Width $\mathfrak{P}$ = 1						
Airplane	21.6399	6.3449	48.7434	0.4924	0.6289	16.137
Peppers	22.7576	11.0071	38.8642	0.6175	0.9129	20.239
Lena	23.4777	10.788	16.1955	1.4819	0.9243	16.754
Girl	23.9204	14.0542	41.2947	0.5812	0.8311	15.101
Couple	25.7891	7.9724	35.6815	0.6726	0.764	5.514
House	20.8773	7.4957	40.366	0.5946	0.6953	19.486
Baboon	19.1288	5.9573	41.4618	0.5788	0.5883	18.971
Sailboat	20.9423	9.4347	33.1817	0.7233	0.7483	23.705

(Continued)

Table 2: Continued

Images	PSNR	SNR	Compression ratio	BPP	Similarity index	File size (KB)
SCHT - RGB at Quantizer Width $\mathfrak{P} = 1$						
SCHT - YCbCr at Quantizer Width $\mathfrak{P} = 1$						
Airplane	4.404	−10.8909	36.1775	0.6634	−0.0481	21.742
Peppers	7.0843	−4.6662	46.8532	0.5122	0.1829	16.788
Lena	9.1208	−3.5688	21.7076	1.1056	0.5546	12.493
Girl	6.5817	−3.2846	52.332	0.4586	0.1854	11.916
Couple	17.0357	−0.781	36.4281	0.6588	0.2122	5.401
House	5.1026	−8.279	35.1808	0.6822	0.0199	22.358
Baboon	6.7729	−6.3986	38.582	0.6221	0.0555	20.387
Sailboat	6.4455	−5.0621	28.7742	0.8341	0.1473	27.336

Table 3: Performance of RGB, CIE La*b*; and YCbCr color spaces in CS-SCHT with Quantizer Width $\mathfrak{P} = 1$

Images	PSNR	SNR	Compression ratio	BPP	Similarity index	File size (KB)
CS-SCHT - RGB at Quantizer Width $\mathfrak{P} = 1$						
Airplane	36.3112	11.6457	31.2355	0.7684	0.8392	25.182
Peppers	37.2743	15.3078	29.9179	0.8022	0.957	26.291
Lena	37.5864	14.7224	11.7288	2.0462	0.9591	23.122
Girl	37.1093	17.8092	30.0859	0.7977	0.8935	20.727
Couple	36.8048	10.1939	32.2538	0.7411	0.8077	30.51
House	35.0999	12.1256	25.1566	0.954	0.8768	31.267
Baboon	32.9466	8.8279	17.6215	1.362	0.7603	44.637
Sailboat	36.3835	13.0788	23.9043	1.004	0.8787	32.905
CS-SCHT – CIE La*b*; at Quantizer Width $\mathfrak{P} = 1$						
Airplane	21.5916	6.2966	47.2444	0.508	0.6281	16.649
Peppers	22.7788	11.0283	40.1415	0.5979	0.9134	19.595
Lena	23.4814	10.7918	16.6499	1.4415	0.9256	16.288
Girl	23.6504	13.7842	36.6237	0.6553	0.8265	17.027
Couple	25.7716	7.9549	38.0263	0.6311	0.7627	5.174
House	20.9025	7.5209	40.8015	0.5882	0.6965	19.278
Baboon	19.1382	5.9667	42.1393	0.5695	0.5884	18.666
Sailboat	20.9082	9.4006	33.3449	0.7198	0.7469	23.589
CS-SCHT - YCbCr at Quantizer Width $\mathfrak{P} = 1$						
Airplane	4.4052	−10.8897	38.4068	0.62449	−0.0476	20.48
Peppers	7.092	−4.6585	50.9801	0.4708	0.1843	15.49
Lena	9.1269	−3.5628	22.1165	1.0852	0.556	12.262
Girl	6.5831	−3.2832	54.4478	0.4408	0.1862	11.453

(Continued)

Table 3: Continued

CS-SCHT - RGB at Quantizer Width $\mathfrak{P} = 1$						
Images	PSNR	SNR	Compression ratio	BPP	Similarity index	File size (KB)
Couple	17.0328	−0.7839	40.684	0.5899	0.2126	4.836
House	5.1049	−8.2766	36.3128	0.6609	0.0201	21.661
Baboon	6.7767	−6.3948	40.6413	0.5905	0.0553	19.354
Sailboat	6.4522	−5.0554	29.8306	0.8045	0.149	26.368

Table 4: Performance of RGB, CIE La*b*; and YCbCr color spaces in NCHT with Quantizer Width $\mathfrak{P} = 1$

NCHT - RGB at Quantizer Width $\mathfrak{P} = 1$						
Images	PSNR	SNR	Compression ratio	BPP	Similarity index	File size (KB)
Airplane	35.7336	11.0596	32.5164	0.7381	0.8237	24.19
Peppers	36.8104	14.8124	31.2578	0.7678	0.9524	25.164
Lena	36.9171	14.0614	12.5512	1.9122	0.9529	21.607
Girl	36.5061	17.2969	31.7899	0.755	0.8828	19.616
Couple	36.2592	9.5682	33.0169	0.7269	0.7819	5.959
House	34.4914	11.4777	25.4777	0.942	0.8589	30.873
Baboon	32.4756	8.0271	18.3753	1.3061	0.7205	42.806
Sailboat	35.9158	12.4427	24.8146	0.9672	0.8619	31.698
NCHT – CIE La*b*; at Quantizer Width $\mathfrak{P} = 1$						
Airplane	21.1197	5.8247	57.8873	0.4146	0.6102	13.588
Peppers	22.2674	10.5169	44.3764	0.5408	0.9501	17.725
Lena	22.8861	10.1964	21.9946	1.0912	0.9163	12.33
Girl	23.5809	13.7147	41.2019	0.5825	0.8187	15.135
Couple	25.1451	7.3284	43.9857	0.5456	0.7322	4.473
House	20.5233	7.1418	48.7706	0.4921	0.6811	16.128
Baboon	18.8209	5.6494	55.4314	0.433	0.5676	14.19
Sailboat	20.3	8.7925	43.3063	0.5542	0.7241	18.163
NCHT - YCbCr at Quantizer Width $\mathfrak{P} = 1$						
Airplane	4.4048	−10.8902	40.7402	0.5891	−0.0482	19.307
Peppers	7.0866	−4.6639	52.3753	0.4582	0.1829	15.018
Lena	9.1242	−3.5655	27.1519	0.8839	0.5542	9.988
Girl	6.5825	−3.2838	59.2148	0.4053	0.1841	10.531
Couple	17.0173	−0.7994	44.1733	0.5433	0.2051	4.454
House	5.1023	−8.2793	44.0361	0.545	0.0193	17.862
Baboon	6.7688	−6.4027	46.7446	0.5134	0.0528	16.827
Sailboat	6.448	−5.0596	34.7257	0.6911	0.1473	22.651

Table 5: Performance of RGB, CIE La*b*; and YCbCr color spaces in UCHT with Quantizer Width $\mathfrak{P}$ =1

Images	PSNR	SNR	Compression ratio	BPP	Similarity index	File size (KB)
UCHT - RGB at Quantizer Width $\mathfrak{P} = 1$						
Airplane	32.6411	−0.6915	11.3283	2.1186	0.2619	69.434
Peppers	33.0455	3.3841	11.8017	2.0336	0.5306	66.649
Lena	30.82	3.3459	4.4748	5.3633	0.5619	60.604
Girl	33.5953	4.0152	8.2676	2.9029	0.3758	75.426
Couple	34.0472	−4.9058	9.3095	2.578	0.1837	21.134
House	32.1243	2.1504	12.2443	1.9601	0.3828	64.24
Baboon	31.6046	3.0631	12.7514	1.8821	0.5019	61.685
Sailboat	33.5901	3.4428	11.0838	2.1653	0.4619	70.966
UCHT – CIE La*b*; at Quantizer Width $\mathfrak{P} = 1$						
Airplane	8.7647	−6.5302	6.2152	3.8615	−0.0131	126.556
Peppers	8.8803	−2.8702	6.5642	3.6562	0.4399	119.828
Lena	8.5668	−4.1229	2.1488	11.1689	0.4069	126.205
Girl	7.0118	−2.8545	5.0531	4.7496	0.1407	123.408
Couple	5.2172	−12.5995	5.8654	4.0918	0.0599	33.544
House	8.4109	−4.9707	6.3308	3.791	0.1229	124.246
Baboon	7.4989	−5.6726	6.2368	3.8481	0.1662	126.118
Sailboat	7.3806	−4.127	6.1724	3.8883	0.1034	127.433
UCHT - YCbCr at Quantizer Width $\mathfrak{P} = 1$						
Airplane	6.2664	−9.0285	8.3154	2.8862	−0.0799	94.592
Peppers	8.1132	−3.6373	5.5064	4.3585	0.1226	142.846
Lena	10.6494	−2.0403	2.4169	9.93	0.4296	112.206
Girl	7.8134	−2.0529	4.8775	4.9206	0.0729	127.581
Couple	13.2799	−4.5368	6.4501	3.7209	0.082	30.503
House	6.8252	−6.5563	6.1479	3.9038	−0.0185	127.941
Baboon	8.4559	−4.7156	6.1809	3.8829	0.0026	127.259
Sailboat	8.0986	−3.409	6.4055	3.7468	0.0434	122.796

Table 6: Performance of RGB, CIE La*b*; and YCbCr color spaces in DOTCHT with Quantizer Width $\mathfrak{P} = 1$

DOTCHT - RGB at Quantizer Width $\mathfrak{P} = 1$						
Images	PSNR	SNR	Compression ratio	BPP	Similarity index	File size (KB)
Airplane	43.5462	18.8405	23.9072	1.0039	0.946	32.901
Peppers	42.4914	21.45842	22.7478	1.055	0.9878	34.578
Lena	43.5679	20.6524	8.4164	2.8516	0.9879	32.222
Girl	43.1586	24.1432	20.0757	1.1955	0.9667	31.062
Couple	43.5503	16.5724	22.9016	1.048	0.9432	8.591
House	41.9567	19.2849	18.495	1.2977	0.9689	42.529
Baboon	38.9102	15.8187	11.1877	2.1452	0.9526	70.307
Sailboat	41.7226	19.8568	17.2501	1.3913	0.9664	45.598
DOTCHT – CIE La*b*; at Quantizer Width $\mathfrak{P} = 1$						
Airplane	27.9953	12.7003	27.7627	0.8645	0.8567	28.332
Peppers	28.2475	16.497	25.102	0.9561	0.9669	31.335
Lena	28.827	16.1373	9.2999	2.5807	0.9699	29.161
Girl	29.4265	19.5602	22.2862	1.0769	0.9355	27.981
Couple	31.0457	13.229	23.622	1.016	0.9168	8.329
House	26.6598	13.2783	21.9694	1.0924	0.8964	35.803
Baboon	23.3112	10.1397	14.3459	1.673	0.8313	54.829
Sailboat	26.0242	14.5167	19.7393	1.2158	0.9056	39.848
DOTCHT - YCbCr at Quantizer Width $\mathfrak{P} = 1$						
Airplane	4.416	−10.8789	16.2834	1.4739	−0.0436	48.305
Peppers	7.0711	−4.6794	31.8051	0.7546	0.1802	24.731
Lena	9.1248	−3.5649	11.2622	2.131	0.5567	24.08
Girl	6.5851	−3.2812	29.0218	0.827	0.2004	21.487
Couple	17.1161	−0.7006	14.7642	1.6256	0.2674	13.326
House	5.1084	−8.2731	17.4294	1.377	0.0243	45.129
Baboon	6.7729	−6.3986	9.0938	2.6391	0.0753	86.495
Sailboat	6.4295	−5.0781	13.1565	1.8242	0.1451	59.786

Table 7: Performance of RGB, CIE La*b*; and YCbCr color spaces in DFT with Quantizer Width $\mathfrak{P} = 1$

DFT - RGB at Quantizer Width $\mathfrak{P} = 1$						
Images	PSNR	SNR	Compression ratio	BPP	Similarity index	File size (KB)
Airplane	36.3767	11.7087	30.8399	0.7782	0.8401	25.505
Peppers	37.3	15.3178	29.3914	0.8166	0.957	26.762

(Continued)

Table 7: Continued

DFT - RGB at Quantizer Width $\mathfrak{P} = 1$						
Images	PSNR	SNR	Compression ratio	BPP	Similarity index	File size (KB)
Lena	37.6126	14.7991	11.398	2.1056	0.9599	23.793
Girl	37.1203	17.8373	28.8126	0.833	0.8941	21.643
Couple	36.8468	10.2184	31.8054	0.7546	0.8077	6.186
House	35.1532	12.1928	24.6714	0.9728	0.8776	31.882
Baboon	32.9705	8.9024	17.2286	1.393	0.7635	45.655
Sailboat	36.3943	13.1344	23.6024	1.0168	0.8798	33.326
DFT – CIE La*b*; at Quantizer Width $\mathfrak{P} = 1$						
Airplane	21.4094	6.1144	54.7905	0.438	0.6284	14.356
Peppers	22.7409	10.9904	41.9237	0.5725	0.9129	18.762
Lena	23.4534	10.7638	17.8135	1.3473	0.9256	15.224
Girl	23.8298	13.9636	45.4314	0.5283	0.8325	13.726
Couple	25.8306	8.0139	39.635	0.6055	0.7661	4.964
House	20.9056	7.5241	44.7221	0.5366	0.698	17.588
Baboon	19.1974	6.0259	43.3995	0.553	0.5927	18.124
Sailboat	20.7947	9.2871	38.2909	0.6268	0.7464	20.542
DFT - YCbCr at Quantizer Width$\mathfrak{P} = 1$						
Airplane	4.405	−10.8899	37.6422	0.6376	−0.0478	20.896
Peppers	7.0961	−4.6544	51.3831	0.4671	0.1846	15.308
Lena	9.1336	−3.556	21.4687	1.1179	0.5568	12.632
Girl	6.5838	−3.2825	54.1641	0.4431	0.1868	11.513
Couple	17.0341	−0.7826	41.5958	0.577	0.2128	4.73
House	5.1057	−8.2758	36.1975	0.663	0.0202	21.73
Baboon	6.7801	−6.3914	40.9013	0.5868	0.0554	19.231
Sailboat	6.4538	−5.0538	30.108	0.7971	0.1489	26.125

Table 8: Performance of RGB, CIE La*b*; and YCbCr color spaces in DCT with Quantizer Width $\mathfrak{P} = 1$

DCT - RGB at Quantizer Width $\mathfrak{P} = 1$						
Images	PSNR	SNR	Compression ratio	BPP	Similarity index	File size (KB)
Airplane	31.5463	5.1981	56.6695	0.4235	0.6336	13.88
Peppers	32.2662	9.2326	44.7704	0.5361	0.8598	17.569
Lena	31.3713	8.3534	19.1832	1.2511	0.8577	14.137
Girl	31.5159	10.7964	47.5842	0.5044	0.5894	13.105
Couple	31.7516	4.0641	59.1545	0.4057	0.5093	3.326
House	31.1968	6.4052	46.8616	0.5121	0.5535	16.785
Baboon	31.398	4.7909	47.3496	0.5069	0.5097	16.612
Sailboat	31.8184	8.0378	40.2771	0.5959	0.6333	19.529

(Continued)

Table 8: Continued

Images	PSNR	SNR	Compression ratio	BPP	Similarity index	File size (KB)
DCT - RGB at Quantizer Width $\mathfrak{P} = 1$						
DCT – CIE La*b*; at Quantizer Width $\mathfrak{P} = 1$						
Airplane	8.1418	−7.1531	132.1526	0.1816	−0.0323	5.952
Peppers	12.4454	0.6949	82.2	0.292	0.4303	9.569
Lena	11.5368	−1.1529	34.1984	0.7018	0.4845	7.93
Girl	11.5914	1.7251	92.9623	0.2582	0.2728	6.708
Couple	16.4031	−1.4136	85.9913	0.2791	0.3565	2.288
House	9.8108	−3.5708	160.4921	0.1495	0.1316	4.901
Baboon	12.1546	−1.0168	134.8717	0.1779	0.1219	5.832
Sailboat	10.6447	−0.8629	140.8617	0.1704	0.1372	5.584
DCT - YCbCr at Quantizer Width $\mathfrak{P} = 1$						
Airplane	4.6263	−10.6686	131.2704	0.1828	−0.04	5.992
Peppers	6.8344	−4.9161	45.7655	0.5244	0.1366	17.187
Lena	9.2898	−3.3998	31.4427	0.7633	0.5218	8.625
Girl	7.1064	−2.7598	84.8885	0.2827	0.1096	7.346
Couple	17.4378	−0.3789	100.793	0.2381	0.1549	1.952
House	5.3034	−8.0782	62.5355	0.3838	0.0108	12.578
Baboon	6.8578	−6.3137	59.829	0.4011	0.0524	13.147
Sailboat	6.701	−4.8066	70.4877	0.3405	0.1698	11.159

Average PSNR of all DOTs shown in Fig. 7 illustrates the better performance of SCHT, CS-SCHT, DOTCHT and DFT against the NCHT, UCHT, and DCT for RGB, in CIE La*b*; UCHT and DCT have less quality outcomes as compared to other DOTs whereas in YCbCr color space all DOTs provides almost similar performance.

SCHT RGB and CIE La*b*;: It has been observed that by varying the value of $\mathfrak{P}$ from 1 to 25 PSNR increases along with file size but the compression ratio decreases and BPP also increases whereas in YCbCr PSNR is almost constant. Tab. 2 demonstrates the results of all images with $\mathfrak{P} = 1$.

CS-SCHT RGB and CIE La*b*;: In different experiments, by varying the values of "$\mathfrak{P}$" in increasing order, the simulation results illustrate that the CS-SCHT in RGB and CIELa*b*; color space PSNR, BPP and file size increase with the value of $\mathfrak{P}$ and compression decreases. However, it is found that PSNR is almost equal for YCbCr.

NCHT RGB and CIE La*b*;: For this variant of Complex Hadamard Transform, it is observed in a number of experiments that the PSNR, BPP, SNR and file size is increased with increasing the value of $\mathfrak{P}$ for the quantization matrix but the compression ratio decreases slowly from 32.5 to 22.2 by the varying value of $\mathfrak{P}$ from 1 to 25 respectively. Though for YCbCr color space, PSNR is varied very slightly for the second digit after the decimal, SNR observed with negative values and file size is increased from 19.3 to 73.3 Kb for $\mathfrak{P} = 1$ and 25 respectively. Tab. 4 demonstrates the results of all different images.

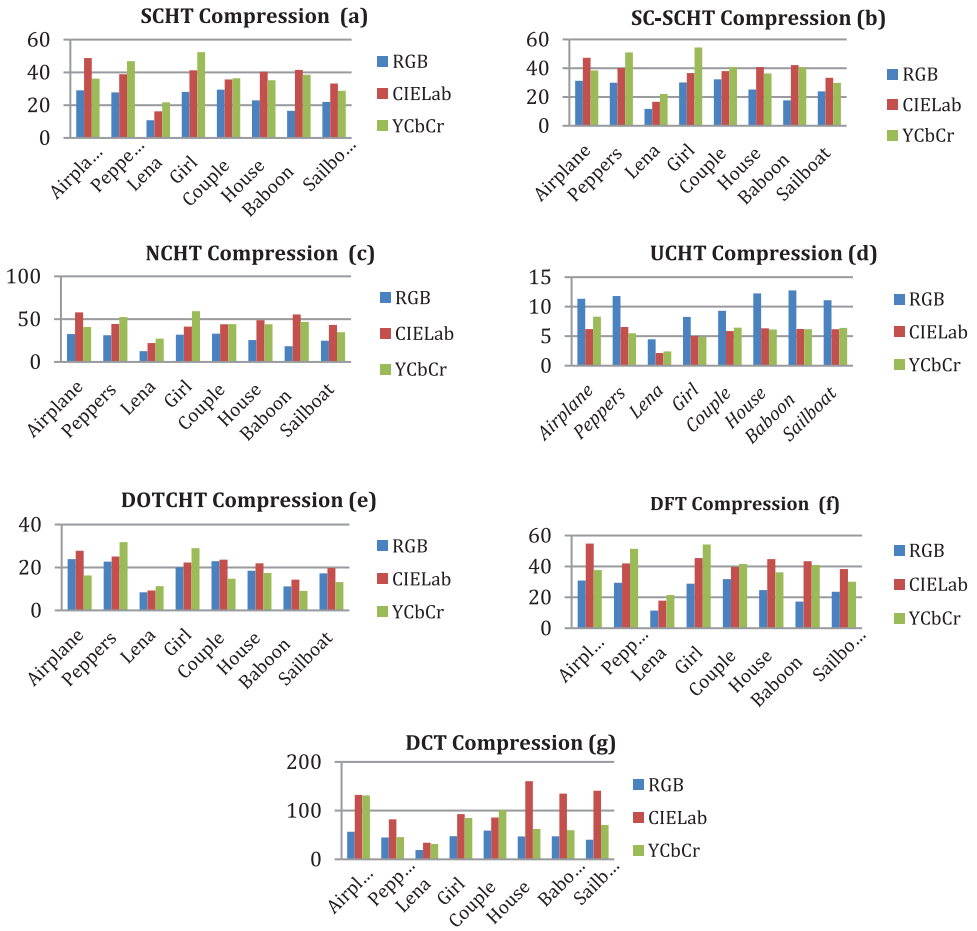

Figure 5: Compression ratio is graphically is presented for RGB, CIE La*b*; and YCbCr color models using (a) SCHT, (b) CS-SCHT, (c) NCHT, (d) UCHT, (e) DOTCHT, (f) DFT and (g) DCT

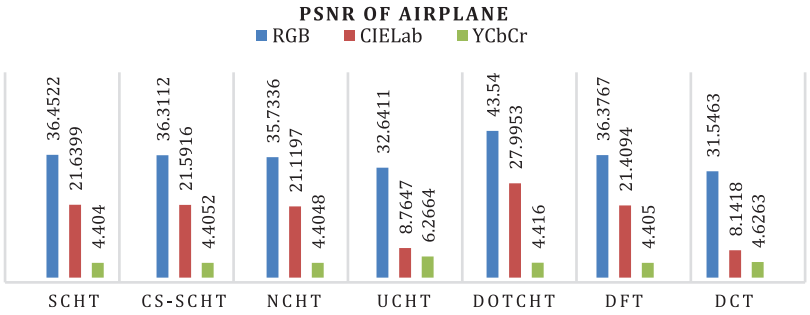

Figure 6: Peak to signal noise ratio at $\mathfrak{P} = 1$ of airplane image for all DOT(s) in different color spaces

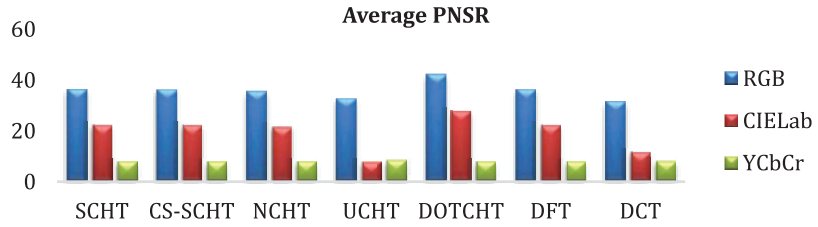

Figure 7: Average peak to signal noise ratio at quantizer width ($\mathfrak{P}$) = 1 for all DOT(s) in different color spaces

UCHT RGB and CIE La*b*;: For various experimentations, by modifying the quantization matrix at different values of "$\mathfrak{P}$" in increasing order, the simulation results illustrate that the UCHT in RGB and CIELa*b*; color space PSNR, BPP and file size increases but compression ratio decreases. SNR in CIE La*b*; shows negative values at lower value of $\mathfrak{P}$ and positive at higher values.

Contrariwise, it is observed that PSNR is an almost same in the YCbCr color domain and SNR is in negative. Tab. 5 presents the results of different parameters for compression using the UCHT.

DOTCHT RGB and CIE La*b*;: Results of DOTCHT in different experiments proves that PSNR, SNR, BPP and file size increases and more or less similarity index shows the same results, but the compression ratio decreases at increasing order of "$\mathfrak{P}$". However, in experimental simulations, changing the value of $\mathfrak{P}$ improves the visual quality. Tab. 6 summarises the qualitative findings.

DFT RGB and CIE La*b*;: It has been observed that different performing parameters of DFT (PSNR, SNR, CR, and SI) possess similarity with SCHT and CS-SCHT due to their similar structure of transformation matrix [29]. Whereas file size of DFT, SCHT, and CS-SCHT [25.2, 27, and 25.2 Kb] to [36.3, 36.1, and 36 Kb] is respectively varied from $\mathfrak{P}$: [1 to 25]. DFT's performance is shown Tab. 7, and the findings can be compared to Tabs. 2 and 3. Fig. 8 depicts these transforms for various test color pictures, CR, and file size.

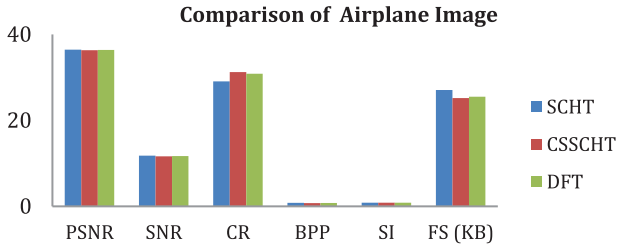

Figure 8: Comparison of airplane image for DFT, SCHT and CSSCHT at quantizer width ($\mathfrak{P}$) = 1 in RGB color space

DCT RGB and CIE La*b*;: DCT performance improves in different experiments. By varying the values of "$\mathfrak{P}$" in increasing order, the simulation results illustrate that the DCT in RGB and CIELa*b*; color space comprises of smaller values of PSNR, SNR, BPP and file size while the compression decreases gradually. However, it is found that PSNR is almost constant for YCbCr.

Fig. 9 shows the difference in bits per pixel and similarity of index during compression with SCHT, CSSCHT, DFT, and DCT in different color planes (a, b and c). Fig. 9d depicts DCT's compression ratio performance in comparison to the other DOTs for an aeroplane image.

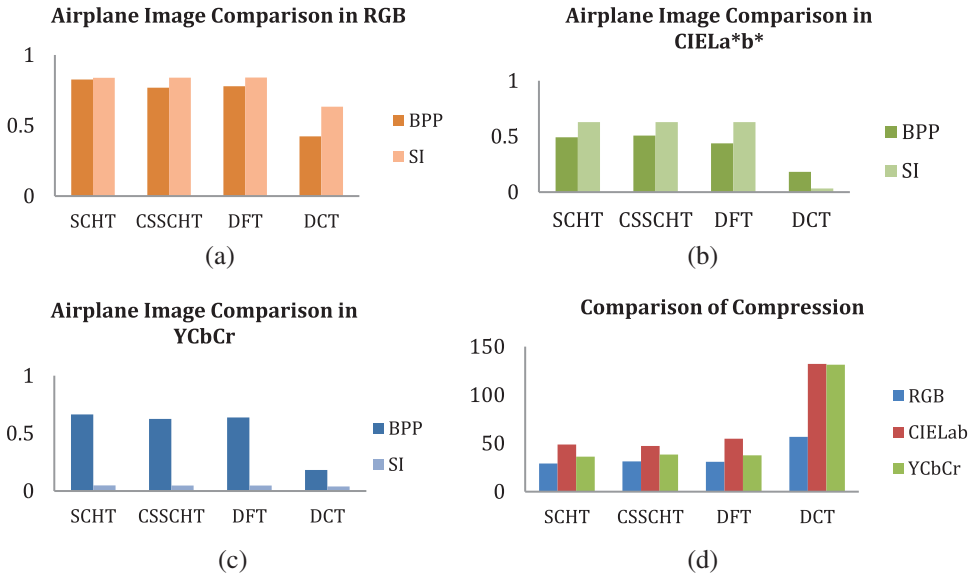

Figure 9: Comparison of airplane image for SCHT, CSSCHT, DFT and DCT: (a) RGB. (b) CIE La*b*;. (c) YCbCr. (d) Comparison of airplane image for SCHT, CSSCHT, DFT and DCT in different color spaces

The performance of DCT in color domain compression study is shown in Tab. 8. Fig. 10 depicts the compressed image quality for DOT(s) in various color spaces. In comparison to other color spaces, the RGB color space has been found to deliver a higher visual quality.

All DOT(s) except the DOTCHT show color artifacts in CIE La*b*;, however the UCHT shows blocky artefacts all across the image. The image quality is not improved by YCbCr since the color information degrades the compressed image. At $\mathfrak{P} = 1$, the image quality of DCT and UCHT compressed images is quite low. The SCHT, CSSCHT, DOTCHT, DFT, and DCT provide higher image quality in the RGB domain for different values of the $\mathfrak{P}$ for the updated quantization matrix, though the DOTCHT provides superior results in all color domains at $\mathfrak{P} = 1$. The image quality is altered by adjusting the value of the $\mathfrak{P}$.

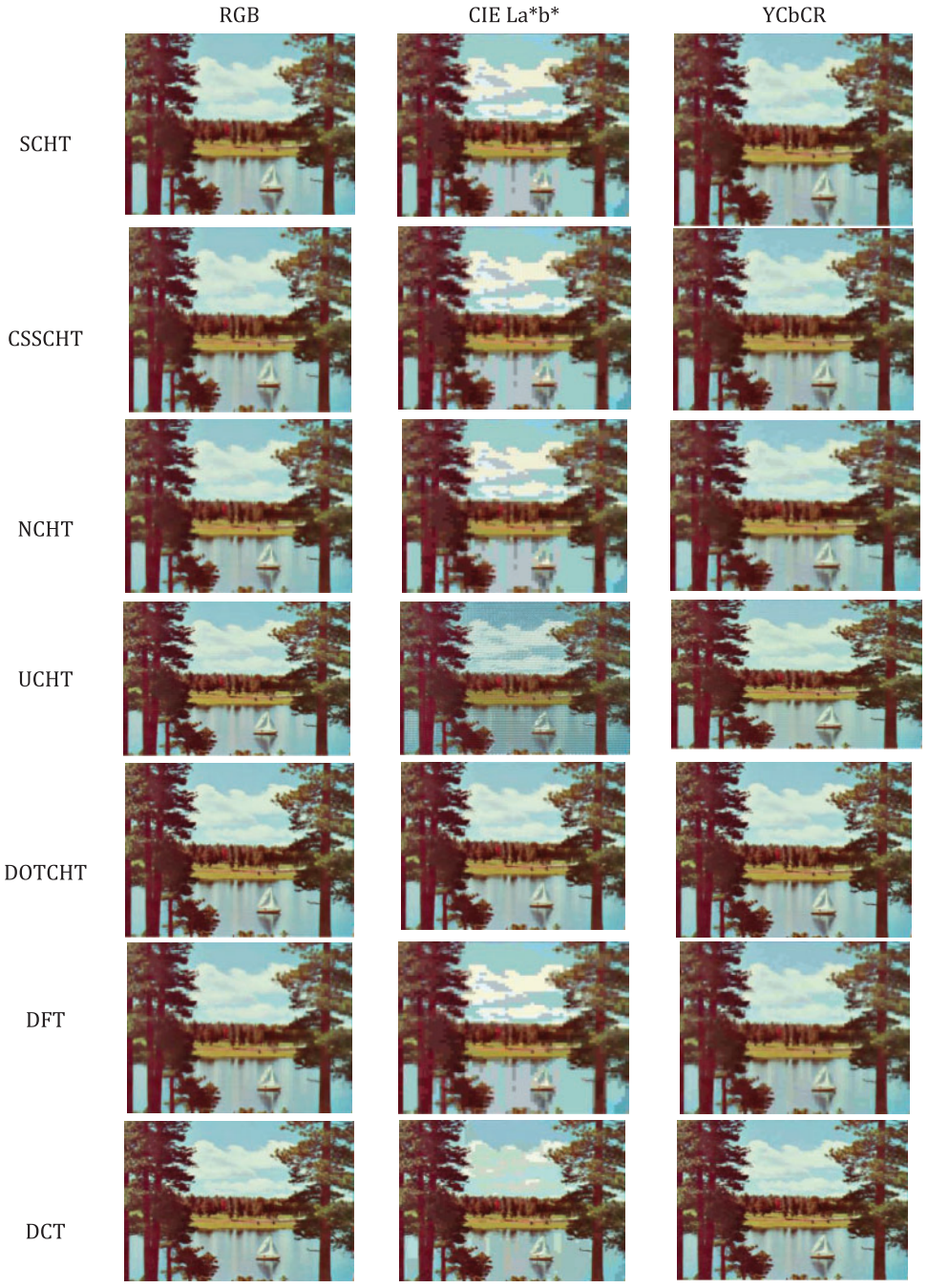

Figure 10: Compressed images of sailboat using DOT(s) in different color spaces

4 Conclusion

In this paper, the qualitative and quantitative analysis is presented in detail. The modified quantization matrix has been applied to several DOT(s) in RGB, YCbCr, and CIE La*b*; color spaces in this research work. This work is based on lossy image compression and is offered for

static color images. The quantization procedure determines the compressed data's quality features. The photos are converted from RGB to CIE La*b*; and YCbCr color spaces before being used. In the transform domain, the color planes are encoded using the proposed quantization matrix. The standard quantization matrix is updated with the corresponding image block to increase the compressed image's efficiency and quality. The thresholding, quantization, de-quantization, inverse Complex Hadamard Transform, CIE Lab, and YCbCr to RGB conversion are among the seven discrete orthogonal transforms performed, which include five variants of the Complex Hadamard Transform, Discrete Fourier Transform, and Discrete Cosine Transform. Peak to signal noise ratio, signal to noise ratio, image similarity index, and compression ratio are used to assess the quality of compressed images. The compressed image quality of each DOT(s) is examined in detail and it has been discovered that the DOTCHT image quality improves when the quantization matrix width is increased. The visual quality of DFT compressed images is comparable to SCHT and CSSCHT. At reduced quantization widths, DCT does not perform better. The compressed image quality degrades when UCHT and NCHT are used. DOTs are playing an increasingly essential role in multimedia applications and advanced devices, helping to cut costs and increase efficiency for multi-purpose needs. We altered the quantization matrix and devised a new adaptive compression technique for color images, lowering the compression ratio and potentially assisting a variety of multimedia applications. In recent years, it has been seen that a variety of online software's have been utilized to connect for meetings, lectures, seminars, and workshops where text, audio, photos, documents, and videos were used for discussion or study purposes due to COVID 19. Because such data requires a large amount of bandwidth, we need approaches that compress these data requirements for faster and more efficient data transfer.

Funding Statement: The authors received no specific funding for this study.

Conflicts of Interest: The authors declare that they have no conflicts of interest to report regarding the present study.

References

[1] M. K. Sardar and A. Adhikari, "A new lossless secret color image sharing scheme with small shadow size," *Journal of Visual Communication and Image Representation*, vol. 68, pp. 102768, 2020.

[2] X. Zeng, S. Tong, Y. Lu, L. Xu and Z. Huang, "Adaptive medical image deep color perception algorithm," *IEEE Access*, vol. 8, pp. 56559–56571, 2020.

[3] S. Mahajan and A. K. Pandit, "Hybrid method to supervise feature selection using signal processing and complex algebra techniques," *Multimedia Tools and Applications*, vol. 5, no. 4, pp. 537, 2021.

[4] M. Yang and A. Sowmya, "An underwater color image quality evaluation metric," *IEEE Transactions on Image Processing*, vol. 24, no. 12, pp. 6062–6071, 2015.

[5] S. Mahajan and A. K. Pandit, "Image segmentation and optimization techniques: A short overview," *Medicon Engineering Themes*, vol. 2, no. 2, pp. 47–49, 2022.

[6] X. R. Zhang, H. L. Wu, W. Sun, A. G. Song and S. K. Jha, "A fast and accurate vascular tissue simulation model based on point primitive method," *Intelligent Automation & Soft Computing*, vol. 27, no. 3, pp. 873–889, 2021.

[7] X. R. Zhang, W. Z. Zhang, W. Sun, H. L. Wu, A. G. Song *et al.,* "A real-time cutting model based on finite element and order reduction," *Computer Systems Science and Engineering*, vol. 43, no. 1, pp. 1–15, 2022.

[8] C. Zhang and X. He, "Image compression by learning to minimize the total error," *IEEE Transactions on Circuits and Systems for Video Technology*, vol. 23, no. 4, pp. 565–576, 2013.

[9] F. Douak, R. Benzid and N. Benoudjit, "Color image compression algorithm based on the DCT transform combined to an adaptive block scanning," *AEU International Journal of Electronics and Communications*, vol. 65, no. 1, pp. 16–26, 2011.

[10] Y. G. Yang, L. Zou, Y. H. Zhou and W. M. Shi, "Visually meaningful encryption for color images by using Qi hyper-chaotic system and singular value decomposition in YCbCr color space," *Optik*, vol. 213, pp. 164422, 2020.
[11] Y. Zhang, L. Yu, M. Sun and X. Zhu, "A mixed radiometric normalization method for mosaicking of high-resolution satellite imagery," *IEEE Transactions on Geoscience and Remote Sensing*, vol. 55, no. 5, pp. 2972–2984, 2017.
[12] G. K. Wallace, "The JPEG still picture compression standard," *IEEE Transactions on Consumer Electronics*, vol. 38, no. 1, pp. xviii–xxxiv, 1992.
[13] C. Wu, J. Chang, C. Quan, X. Zhang and Y. Zhang, "The optical image compression and encryption method based on Fresnel diffraction and discrete wavelet transform," *Results in Optics*, vol. 1, pp. 100021, 2020.
[14] S. H. Farghaly and S. M. Ismail, "Floating-point discrete wavelet transform-based image compression on FPGA," *AEU International Journal of Electronics and Communications*, vol. 124, pp. 153363, 2020.
[15] Y. Hou, Z. Ren, Y. Tao and W. Chen, "Learning-based parameter prediction for quality control in three-dimensional medical image compression," *Frontiers of Information Technology & Electronic Engineering*, vol. 22, no. 9, pp. 1169–1178, 2021.
[16] S. T. Ahmed and S. Sankar, "Investigative protocol design of layer optimized image compression in telemedicine environment," *Procedia Computer Science*, vol. 167, pp. 2617–2622, 2020.
[17] S. Yuan and J. Hu, "Research on image compression technology based on Huffman coding," *Journal of Visual Communication and Image Representation*, vol. 59, pp. 33–38, 2019.
[18] D. Venugopal, S. Mohan and S. Raja, "An efficient block based lossless compression of medical images," *Optik*, vol. 127, no. 2, pp. 754–758, 2016.
[19] C. Y. Pang, R. G. Zhou, B. Q. Hu, W. Hu and A. El-Rafei, "Signal and image compression using quantum discrete cosine transform," *Information Sciences*, vol. 473, pp. 121–141, 2019.
[20] A. Aung, B. P. Ng and S. Rahardja, "Sequency-ordered complex Hadamard transform: Properties, computational complexity and cpplications," *IEEE Transactions on Signal Processing*, vol. 56, no. 8, pp. 3562–3571, 2008.
[21] D. Jabeen, G. Monir and F. Azim, "Sequency domain signal processing using complex Hadamard transform," *Circuits, Systems, and Signal Processing*, vol. 35, no. 5, pp. 1783–1793, 2016.
[22] A. Aung, B. P. Ng and S. Rahardja, "Conjugate symmetric sequency-ordered complex Hadamard transform," *IEEE Transactions on Signal Processing*, vol. 57, no. 7, pp. 2582–2593, 2009.
[23] A. Aung and B. P. Ng, "Natural-ordered complex Hadamard transform," *Signal Processing*, vol. 90, no. 3, pp. 874–879, 2010.
[24] S. Rahardja and B. J. Falkowski, "Family of unified complex Hadamard transforms," *IEEE Transactions on Circuits and Systems II: Analog and Digital Signal Processing*, vol. 46, no. 8, pp. 1094–1100, 1999.
[25] S. Pei, C. Wen and J. Ding, "Conjugate symmetric discrete orthogonal transform," *IEEE Transactions on Circuits and Systems II: Express Briefs*, vol. 61, no. 4, pp. 284–288, 2014.
[26] J. G. Proakis and D. G. Manolakis, *Digital Signal Processing: Principles, Algorithms, and Applications*, 4th ed., Hoboken: Prentice-Hall, 2007.
[27] K. R. Rao, D. H. Ochoa and S. Shreyanka, "3 The discrete cosine and sine transforms," in *JPEG Series*. Denmark: River Publishers, pp. 49–65, 2021.
[28] C. Connolly and T. Fleiss, "A study of efficiency and accuracy in the transformation from RGB to CIELAB color space," *IEEE Transactions on Image Processing*, vol. 6, no. 7, pp. 1046–1048, 1997.
[29] A. A. Siddique, M. T. Qadri and Z. Mohy-Ud-Din, "Exhaustive crisp parameter modification in quantization table for effective image compression," *Mehran University Research Journal of Engineering and Technology*, vol. 39, no. 2, pp. 279–286, 2020.